Targeting prostate cancer by new bispecific monocyte engager directed to prostate-specific membrane antigen

Gargi Das[1,2], Jakub Ptacek[1], Barbora Havlinova[1], Jana Nedvedova[1], Cyril Barinka[1], and Zora Novakova[1]*

[1] Laboratory of Structural Biology, Institute of Biotechnology of the Czech Academy of Sciences, Vestec, Czech Republic.

[2] Department of Cell Biology, Faculty of Natural Science, Charles University, Prague, Czech Republic.

*Corresponding author: Zora Novakova, email zora.novakova@ibt.cas.cz, Tel: +420 325 873 736

Keywords: prostate cancer; glutamate carboxypeptidase II; antibody engineering; bispecific engager; immunotherapy; prostate specific membrane antigen (PSMA); antibody-dependent cell-mediated phagocytosis

Abstract

Prostate cancer (PCa) ranks as the second leading cause of cancer-related deaths among men in the United States. Prostate-specific membrane antigen (PSMA) represents a well-established biomarker of PCa and its levels correlate positively with the disease progression, culminating at the stage of metastatic castration-resistant prostate cancer. Due to its tissue-specific expression and cell surface localization, PSMA shows superior potential for precise imaging and therapy of PCa. Antibody-based immunotherapy targeting PSMA offers the promise of selectively engaging the host immune system with minimal off-target effects.

Here we report on the design, expression, purification, and characterization of a bispecific engager, termed 5D3-CP33, that efficiently recruits macrophages to the vicinity of PSMA-positive cancer cells mediating PCa death. The engager was engineered by fusing the anti-PSMA 5D3 antibody fragment to a cyclic peptide 33 (CP33) selectively binding the Fc gamma receptor I (FcγRI/CD64) on the surface of phagocytes. Functional parts of 5D3-CP33 engager revealed nanomolar affinity for PSMA and FcγRI/CD64 with dissociation constants of K_D = 3 nM and K_D = 140 nM, respectively. At a concentration as low as 0.3 nM, the engager was found to trigger production of reactive oxygen species by U937 monocytic cells in the presence of PSMA-positive cells. Moreover, flow cytometry analysis demonstrated antibody-dependent cell-mediated phagocytosis of PSMA-positive cancer cells by U937 monocytes when exposed to 0.1 nM 5D3-CP33. Our findings illustrate that 5D3-CP33 effectively and specifically activates monocytes upon PSMA-positive target engagement, resulting in the elimination of tumor cells. The 5D3-CP33

41 engager can thus serve as a promising lead for the development of new immunotherapy tools for

42 the efficient treatment of PCa.

Introduction

Prostate cancer (PCa) remains one of leading causes of death amongst men. According to cancer statistics 2023, PCa alone accounts for 29% of newly diagnosed cases and 12% of cancer-related deaths **[1]**. Hence, PCa management is one of the pressing unmet medical needs.

Prostate specific membrane antigen (PSMA, EC 3.4.17.21), also known as glutamate carboxypeptidase II (GCPII), is an established PCa biomarker. PSMA is a 100 kDa type-II transmembrane protein with a large extracellular part that can be readily targeted by both small-molecule ligands as well as macromolecules and nanoparticles **[2-6]**. While PSMA is at low levels present in several healthy tissues including brain, kidney, salivary glands, prostate, and small intestine, PSMA expression levels are markedly increased in all stages of PCa, with the highest expression observed in metastatic androgen resistant PCa **[7-11] [12-14].** Altogether, highly specific, and abundant expression makes PSMA an ideal target for PCa imaging and therapy **[15-19].**

Owing to the success of immunotherapy targeting various hematological malignancies, immunotherapy approaches are now researched and utilized as treatment strategies against solid tumors, including prostate cancer **[20-23]**. For example, Sipuleucel-T, a cell-based vaccine exploiting patients' autologous dendritic cells loaded with prostatic acid phosphatase, was approved by the FDA in 2010 for the treatment of metastatic castrate-resistant hormone-refractory PCa **[24, 25].** Furthermore, several viral-based vaccines, including PROSTVAC, CV301, and Ad5-PSA, that trigger an immune response directed at PCa antigens are under investigation **[26-29]**. Yet another therapeutic approach involves blocking inhibitory signals for cytotoxic T-

cells, as exemplified by Ipilimumab that attenuates CTLA-4 function, enhancing thus the PCa antitumor effect of T-cells **[30, 31]**.

Monoclonal antibodies (mAb) targeting PSMA also attract current interest in the PCa field since they might offer superior specificity against PSMA compared to small molecule inhibitors [32]. mAbs can directly block proliferation of tumor cells **[33]** when applied as carriers of cytotoxic payloads. Moreover, they can elicit the host immune system to execute anti-tumor activity via cell-dependent cytotoxicity (CDC) or antibody-dependent cell-mediated phagocytosis (ADCP) **[34-37].** The antibody-dependent activation of the complement pathway is an additional mechanism of eradicating abnormal tumor cells **[38-43]**. Similarly to PSMA-targeted immunotherapeutic strategies, PSMA-radioligand therapy using PSMA-specific antibody loaded with Lutetium-177 (177Lu-J591) was associated with highly significant decrease in prostate specific antigen (PSA) levels in metastatic castration-resistant prostate cancer (mCRPC) patients **[44]**. Furthermore, other mAb-based therapies including CAR T (chimeric antigen T-cell receptor) and BiTE (bispecific T-cell engager) targeting PSMA, are being intensively studied **[45-49]**.

In this study, we report on the development and functional characterization of a bispecific monocyte engager capable of simultaneously targeting PSMA-positive cancer cells and the Fc gamma receptor I (FcγRI/CD64) receptor present on the monocyte/macrophage surface. The PSMA-targeting arm, in the form of the single-chain variable fragment (scFv), has been derived from the 5D3 antibody that revealed picomolar affinity and high specificity for human PSMA **[49, 50]**. The CP33 cyclic peptide reported previously **[51]** was included to form fusion partner that targets FcγRI/CD64 receptors on monocytes/macrophages. In our hands, the 5D3-CP33 engager activated monocytes in the PSMA-dependent manner at concentrations as low as 100 pM leading

to the killing of PSMA-positive cancer cells. The data suggest that the 5D3-CP33 fusion protein can serve as a promising candidate for the development of future immunotherapeutic modalities targeting PCa.

Results

Expression and purification of 5D3/CP33 fusion proteins

5D3/CP33 monocyte engagers were designed using sequences of a single chain 5D3 fragment (scFv HL) and the CP33 sequence that were described previously **[50] [51].** To evaluate the importance of the positioning of PSMA and CD64-targeting arms on expression levels, stability, and affinity of 5D3/CP33 fusions, we constructed two variants of monocyte engagers that differ in the arrangement of 5D3- and CP33-derived sequences. Both variants further harbor the BiP secretion signal and the SA-strep II affinity tag at their N- and C-terminus, respectively (Figs. 1 and S1). Recombinant fusion proteins were heterologously expressed in S2 insect cells and purified from conditioned medium using the combination of Streptactin-XT affinity and size exclusion chromatography. A chimeric 5D3 molecule (ch5D3), comprising 5D3 variable murine domains fused to constant domains of human IgG1, was constructed to serve as a positive functional control (Fig 1C). Chimeric 5D3 was heterologously expressed in HEK293T/F17 cells and purified via protein A affinity chromatography.

Biophysical and functional characterization of 5D3/CP33 constructs

Purity and oligomeric status of purified fusions were evaluated by SDS-PAGE and the analytical size exclusion chromatography, respectively, confirming the presence of monodisperse monomeric proteins with over >95% purity (Fig 1). Next, the thermal stability of constructs was determined using differential scanning fluorimetry (nanoDSF) and a single peak corresponding to the melting temperature of 53.5 ˚C and 51.5 ˚C was observed for the 5D3-CP33 and CP33-5D3 construct, respectively (Fig 1E). nanoDSF analysis confirmed the existence of fully folded 5D3/CP33 fusions and obtained values are in line with melting temperatures reported previously for the 5D3-scFv HL construct **[50].**

Since the 5D3-CP33 fusion revealed slightly higher thermal stability (by 2 ˚C) than CP33-5D3 construct, the former was selected for ensuing functional experiments. Two peaks were observed for the ch5D3, where the first peak at 66.8 ˚C reflected the melting temperature of the Fab fragment, while the second peak at 82.2 ˚C corresponded to the third constant domain (CH3) of human immunoglobulin **[52].**

Fig 1: Biophysical characterization of 5D3 monocyte engagers.

(A, B, C) A single peak in the chromatograms of analytical SEC confirmed a monomeric form of each construct. The schemes of constructs provided on the right side of each chart show arrangement of BiP signal (grey), antibody domains (green), CP33 (beige) and SA-strep II tag (violet; created with BioRender.com). (D) Non-reduced samples separated in SDS PAGE gels stained by Coomassie Brilliant Blue G-250 show >95% purity of all constructs. (E) The thermal stability of each construct was determined using nanoDSF. Melting temperatures of individual

127 constructs were calculated from the first derivative of the fluorescence ratio at 350 nm and 330
128 nm.

129

130 ## Binding affinity of 5D3-CP33 and ch5D3 constructs

131 The binding specificity and affinity of each arm of the 5D3-CP33 fusion and of ch5D3 was
132 determined by flow cytometry using PSMA-positive PC3-PIP cells and FcγRI-positive HEK-293T-
133 CD64 cells together with PC3 and HEK-293T cell lines included as PSMA- and FcγRI-negative
134 controls, respectively. At 100 nM concentration, both 5D3-CP33 and ch5D3 bound selectively to
135 PSMA- and CD64-positive cell lines, while nonsignificant binding was observed for corresponding
136 controls, confirming high selectivity of the constructs for both target antigens (Fig 2).
137 Furthermore, 5-fold dilutions series of the constructs were used to determine binding affinities
138 of individual arms for their respective antigens (Fig 2). For the 5D3 arm, dissociation constants of
139 3.4 nM and 2.9 nM were determined by the binding curve fitting for 5D3-CP33 and ch5D3
140 construct, respectively. Similarly, K_D values of 140.4 and 2.2 nM were calculated for the anti-CD64
141 arms of 5D3-CP33 and ch5D3, respectively (Fig 2).

142

143 **Fig 2: Characterization of purified 5D3-CP33 and ch5D3**.
144 (A) Target specificity of 200 nM 5D3-CP33 to PSMA antigen was determined by flow cytometry
145 using PSMA-positive PC3-PIP cells. PC3 cells served as PSMA-negative control. Approximately
146 30,000 live cells were included in analysis to generate histogram. (B) Specificity of 400 nM 5D3-
147 CP33 to FcγRI/CD64 was estimated on CD64-positive HEK-293T-CD64 cells using flow cytometry.
148 HEK-293T cells served as FcγRI/CD64-negative controls. Approximately 30,000 live cells were

involved in analysis. (C, D) Specific affinity of 5D3-CP33 to PSMA and FcγRI/CD64 was determined by flow cytometry using PC3-PIP cells and HEK-293T-CD64 cells, respectively. PC3 and HEK-293T cells were used as negative controls. (E, F) Estimation of specific affinity of ch5D3 run identically to 5D3-CP33 measurement. Individual K_D values are shown in upper left corner of charts.

Monocyte activation by 5D3-CP33 and ch5D3 constructs

The 5D3-CP33 fusion shall be able to activate monocytes/macrophages via binding to and clustering FcγRI/CD64 receptors on cell surface and the activation status can be determined by quantifying the production of reactive oxygens species (ROS) by FcγRI/CD64-positive cells. U937 monocytic (pre-macrophage) cell line was implemented in cell-based experiments as the FcγRI/CD64-positive cell line, while prostate cancer-derived PC3-PIP and PC3 cells were used as representatives of PSMA-positive and PSMA-negative cells, respectively **[53, 54]**. Prior experiment, U937 monocytes were stimulated by 0.1 mg/mL IFN-γ treatment running for 24 hours to enhance FcγRI receptor levels on the cell surface. The stimulated U937 cells were then mixed with PC3-PIP or PC3 cells in the presence of 5-fold dilution series of the 5D3-CP33 construct (final concentration 200 nM to 0.32 nM), and ROS production was quantified by a lucigenin-based chemiluminescence readout. As shown in Fig 3, we observed a marked increase in ROS production by stimulated U937 cells upon mixing with PSMA-positive PC3-PIP cells in the presence of the 5D3-CP33 fusion even at concentrations as low as 320 pM. At the same time, no detectable ROS production by activated U937 cells was observed in the presence of PSMA-negative PC3 cells or in the absence of the 5D3-CP33 fusion. These results thus confirm that U937 monocytes are selectively activated only upon simultaneous engagement of PSMA and CD64

antigens on the surface of cancer and immune cells, respectively. Similarly, to 5D3-CP33, the ch5D3 construct selectively activated U937 cells only in the presence of PSMA-positive cells, but not in the presence of PSMA-negative controls (Fig 3).

Fig 3: **ROS production driven by 5D3-CP33.**

(A) Production of ROS by activated U937 cells in the presence of 5D3-CP33 or ch5D3 co-cultured with PSMA-positive PC3-PIP cells or PSMA-negative PC3 cells. (B) Quantification of produced ROS was visualized at 4-minute time-point to show in detail the difference between various concentrations of constructs and the ratio of ROS production in the presence of PSMA-positive and PSMA-negative cells. (C) ROS production by activated U937 cells in the presence of serial dilution of 5D3-CP33 co-cultured with PC3-PIP cells or PC3 cells. (D) Visualization at 4-minute time-point shows in detail concentration-dependent effect of 5D3-CP33 on ROS production in the presence of PSMA-positive and negative cells. The level of ROS was measured using the lucigenin-based chemiluminescence assay.

Phagocytosis induced by 5D3-CP33 and ch5D3 constructs

In addition to ROS production, immune cells can eliminate target cancer cells by phagocytosis. To determine whether the 5D3-CP33 fusion can elicit selective phagocytosis of cancer cells managed by monocytes, IFN-γ-stimulated U937 and target PC3/PC3-PIP cancer cells were at first labeled with the DiD and DiO dye, respectively. U937 cells were then mixed with target cells and construct, and co-cultured for 1 hour. Following co-cultivation, phagocytosis was monitored by flow cytometry and confocal microscopy. Flow cytometry two-dimensional dot-plots (Fig 4A)

were engaged to show specific signal arising from U937 cells, and PC3 or PC3-PIP cells, while double positive objects (upper right quadrant of the dot plot) were suggested to present process of engulfing target cells by U937 cells. Flow cytometry analysis revealed that antibody-dependent cell-mediated phagocytosis (ADCP) is only evident under conditions, where U937 cells are co-cultured with PSMA-positive PC3-PIP cells in the presence of 5D3-CP33. In the presence of 111.1 nM 5D3-CP33, approximately 25% of double positive cells correspond to cancer cells being engulfed by stimulated monocytes. To the contrary, a limited number (<2%) of double positive cells is observed in the absence of 5D3-CP33 or when PSMA-negative PC3 cells were used. Fig 4B further shows a positive correlation between the level of ADCP and 5D3-CP33 concentrations ranging from 0.1 nM to 1 µM in U937/PC3-PIP co-cultures revealing that 5D3-CP33 can induce cancer-cell phagocytosis at concentrations as low as 100 pM. Like 5D3-CP33, the ch5D3 construct demonstrated selective phagocytosis by U937 cells exclusively in the presence of PSMA-positive cells, with no activation observed in PSMA-negative controls (Fig 4C). To provide visual confirmation of flow cytometry data, we imaged ADCP in analyzed cell mixtures by confocal microscopy (S2 Fig). The microscopy data revealed co-localization of specific signals arising from U937 cells (red) and target cells (green) and confirmed engulfment of PC3-PIP cells by the activated monocytes, whereas no engulfed objects were observed in U937/PC3 mixtures.

Fig 4: **Antibody-dependent cell-mediated phagocytosis (ADCP) of prostate cancer cells by U937 monocytes.**

(A) PC3/PC3-PIP cells and U937 cells were labeled by DiO and DiD dye, respectively, co-incubated in the presence/absence of 111 nM 5D3-CP33 and analyzed by flow cytometer. Upper right

quadrant of two-dimensional dot-plot charts shows double positive events that represent target cells engulfed by U937 monocytes. (B) U937/PC3-PIP co-cultures revealed positive correlation between the level of ADCP and 5D3-CP33 concentration. (C) The chart shows selective effect of 5 nM ch5D3 on the ADCP level in U937/PC3 and U937/PC3-PIP co-cultures, respectively.

Discussion

Myeloid cells, including monocytes and macrophages, can readily infiltrate the tumor microenvironment (TME) and they constitute a substantial portion (30-50%) of tumor-infiltrating immune cells **[55, 56]**. Macrophages within the TME are referred to as the tumor-associated macrophages (TAMs) and their phenotypes oscillate between M1 tumor suppressive and M2 pro-tumorigenic subtypes.**[57, 58]** TAMs are prevalent in most cancers that reveal poor clinical outcomes **[59, 60]. T**he M2 macrophages promote cancer growth by supporting angiogenesis, metastasis, and directly interfering with effector T-cells at the tumor site **[58, 61].** Significant role of TAMs in tumor physiology provoked the development of therapeutic modalities focusing on these cells to improve clinical outcomes of cancer patients **[55, 62, 63]**. Several small molecules were designed to enhance macrophage anti-tumor activity. As an example, the R848 ligand was used to reprogram TAMs into the M1 tumor-suppressive phenotype thereby potentiating an effect of the ADCP treatment **[64, 65]**. Additionally, small molecule inhibitors of the CCR2 receptor present on macrophages exhibited the potential to enhance chemotherapy effects in models of pancreatic ductal adenocarcinoma **[66]**.

Inspired by the success of the chimeric antigen receptor T-cell (CAR-T) in leukemia treatment, CAR-macrophages engineered for the immunotherapy of solid tumors have garnered attention in recent years **[67-70]**. CAR-macrophages, advantageously derived from patients' inducible pluripotent stem cells (iPSCs) **[71, 72]**, are able to convert M2 macrophages to the M1 tumor-suppressive phenotype without reverse transformation **[73]**. These cells can support cytotoxicity of T-cells by generation of proinflammatory signals and upregulation of MHC and TNF expression **[74]**. This study aimed to reveal an alternative macrophage-mediated immunotherapy that simultaneously engaged FcγRI/CD64 receptors and prostate-specific membrane antigen present on the surface of host macrophages and prostate cancer cells, respectively. The 5D3/CP33 bispecific macrophage engagers were designed to eradicate tumor cells via host immune cells without need of technically challenging and economically demanding engineering of personalized CAR-macrophages.

Direct comparison of the 5D3/CP33 engager with the full length chimeric 5D3 antibody could make the estimation of their performance *in vitro* more accurate. Both the CP33 peptide and the antibody crystallizable fragment (Fc) bind to overlapping epitopes on FcγR receptors, with the former being strictly selective for FcγRI over other FcγR variants **[51].** At the same time, an apparent affinity of CP33 for FcγRI is approximately 63-fold lower than affinity of Fc part of the intact antibody (140.4 *vs* 2.2 nM, respectively; our data and ref **[51]**). Despite its markedly lower, mid-nanomolar FcγRI affinity, the 5D3/CP33 engager can still elicit macrophage activation (ROS production, phagocytosis) at picomolar concentrations *in vitro*. The ability of the 5D3/CP33 engager to mediate targeted elimination of PSMA-positive cancer cells at particularly low concentrations would be beneficial *in vivo*, where lower dosage can minimize adverse

immunogenic effects such as the anti-drug antibody (ADA) response or the cytokine release syndrome **[75, 76].** Additionally, small molecular size of the 5D3/CP33 fusion (35 kDa) compared to the full-length antibody (150 kDa) can be advantageous due to better penetrability in the solid tumor micro-environment **[77, 78].** On the other hand, the longer circulation time of the full-length antibody may be preferable for higher therapeutic efficacy **[79-83]**. It is obvious that optimal fine-tuned functional characteristics of the engager can only be determined in (pre)clinical settings and might require engineering of 5D3/CP33 variants with extended serum half-lives and increase stability *in vivo* **[84-87].**

In 2014, McEnaney and colleagues reported on a synthetic antibody mimic targeting prostate cancer (SyAM-P) representing a fully synthetic small-molecule fusion of CP33 **[88].** PSMA-binding arm of the molecule was derived from an urea-based scaffold currently used in clinic for prostate cancer imaging and therapy **[89]**. Additional improvement of effector functions came with the construction of multivalent derivatives. In case of SyAM-P as well as 5D3/CP33, affinity of the CP33 part for monocytes was found to be considerably low when compared to the affinity of PSMA-binding arm. However, the difference might carry benefits in limited binding to monocyte surface receptors in the absence an antigen, minimizing thus potential off-target effects **[90]**. Interestingly, replacing of the urea-based scaffold of SyAM-P by 5D3-scFv in the 5D3/CP33 engager has the potential to further mitigate off-target effects of the engager as the urea-based ligands were reported to engage other physiological targets, including glutamate carboxypeptidase III, NAALAdase L (PSMA paralogs) and the mGluR8 receptor **[32, 91].**

Conclusions

We developed a novel 5D3-CP33 engager with potential to mediate targeted eradication of PSMA-positive prostate cancer cells by cells of the host immune system. Picomolar concentrations of the engager efficiently activate monocytes *in vitro* and elicit killing of target cancer cells by the combination of reactive oxygen species production and phagocytosis. Our data thus encourage further optimization and investigations including *in vivo* testing, moreover, the engager is suggested to serve as a promising candidate for the development of future immunotherapeutic modalities targeting prostate cancer and other solid tumors expressing the PSMA antigen.

Materials and Methods

Chemicals and reagents

The chemicals and reagents were purchased from Sigma-Aldrich (Steinheim, Germany) unless stated otherwise. The restriction enzymes and ligases were purchased from New England Biolabs (Ipswich, MA, USA).

Cell culture and cell lines

PC3-PIP and PC3 cell lines were kindly provided by Dr. Warren Heston (Cleveland Clinic, Cleveland, OH, USA) [9], LNCaP cells were generously provided by Dr. Zdenek Hodny (Institute of

297 Molecular Genetics, Prague, Czech Republic), and and suspension culture of HEK-293T cells was
298 kindly donated by Dr. Ondrej Vanek (Faculty of Science, Charles University, Prague, Czech
299 Republic). U937, DU145 and adherent HEK-293T cell lines were acquired from the American Type
300 Culture Collection (ATCC, USA). PC3-PIP, PC3, LNCaP, U937 and DU145 cells were maintained in
301 RPMI-1640 media, whereas adherent HEK-293T cell lines cells were cultivated in Dulbecco's
302 Modified Eagle media. Both cultivation media were supplemented with 10% v/v fetal bovine
303 serum (FBS; Gibco, Life Technologies, Carlsbad, CA) and 2 mM L-glutamine (Life Technologies,
304 Thermo Fisher Scientific, Carlsbad, CA, USA). and cells were maintained at 37 °C under 5% CO2
305 atmosphere. Suspension culture of HEK-293T cells was cultivated in the 1:1 mixture of FreeStyle
306 F17 (Gibco) and EX-CELL 293 media. Insect Drosophila melanogaster Schneider S2 cells were
307 cultivated at 26°C in Insect-XPRESS media (Lonza, Basel, Switzerland) supplemented with 2 mM
308 L-glutamine.

309 ## Construction of 5D3/CP33 fusions

310 Two variants of monocyte engagers were created in this study. In 5D3-CP33 variant, 5D3-scFv
311 HL (heavy-light chain) was fused to the N-terminus of CP33 **[51],** while design of CP33-5D3 variant
312 contained opposite order of functional parts. The 5D3-scFv-CP33 gene string and the opposite
313 variant were amplified by PfuUltra II Hotstart PCR Master Mix (Agilent, Santa Clara, CA, USA)
314 using 0.8 µM primers specified in S1 Table. The amplification program started by initial
315 denaturation (95 °C for 2 min) followed by 25 cycles of denaturation (95 °C for 30 s), annealing
316 (60 °C for 30 s) and extension (72 °C for 1 min) finalized by extension at 72 °C for 10 min. Amplified
317 sequences were digested using BglII and XhoI enzymes, and the digested products were ligated

into the backbone vector pMT/BiP/V5-HisA. Final plasmids obtained were termed pMT/BiP/5D3-CP33 and pMT/BiP/CP33-5D3, representing the 5D3-CP33 and CP33-5D3 fusions, respectively.

Construction of chimeric 5D3

Variable domains of 5D3 mAb and backbone of expression vector pVITRO1-dV-IgG1/κ (a gift from Andrew Beavil; Addgene plasmid #52213)[92] were amplified by Phusion Flash High-Fidelity PCR Master Mix (Thermo Fisher Scientific) using primers specified in Table S1. Amplification of 0.5 µg template started by initial denaturation (98 °C for 10 sec) followed by 25 cycles of denaturation (98 °C for 1 s), annealing (60 °C for 5 s) and extension (72 °C for 75 sec) and finalized by extension at 72 °C for 1.5 min. PCR products purified by GenElute PCR Clean-Up Kit (Sigma-Aldrich) were mixed in molar ratio 1:1 and 0.37 pmol of total DNA was then treated by Gibson Assembly Master Mix (New England Biolabs) for 3 hours at 50°C. Assembled molecules were transformed into XL1-Blue competent cells (Agilent) and final expression plasmid was isolated using QIAGEN Plasmid Midi Kit (Qiagen, Hilden, Germany).

Stable overexpressing cell lines

pMT/BiP/5D3-CP33 and pMT/BiP/CP33-5D3 expression vectors were transfected into S2 cells together with the selection plasmid pCoBLAST (Invitrogen) as described earlier**[50]**. Transfected cultures were selected using 40 µg/mL blasticidine (InvivoGen, San Diego, CA, USA) until stably transfected cell population was established.

Expression plasmid carrying gene of human FcγRI/CD64 receptor (pCDNA4-CD64) was kindly provided by Pavel Sacha (Institute of Organic Chemistry and Biochemistry, Prague, Czech Republic). The vector was introduced into adherent HEK-293T cells using JetPRIME transfection reagent (Polyplus, Illkirch, France). FcγRI/CD64-positive cells were selected in media containing 50 µg/mL Zeocin (InvivoGen). Single-cell colonies were isolated using cloning discs and further continuously cultivated in the presence of 50 µg/mL Zeocin.

Expression and purification of constructs

Monocyte engagers were over-expressed by stably transfected S2 cells in 7 days upon induction by 0.7 mM CuSO4. The conditioned media was then harvested, filtered by tangential flow filtration (Sartoflow Smart, Sartorius Stedim Systems GmbH, Guxhagen, Germany), and purified by streptactin-XT affinity purification according to the established protocol **[50].** Further, eluted fractions from the affinity chromatography column were subjected to size exclusion chromatography (SEC) using an Enrich 70 10/300 column (GE Healthcare Biosciences, Uppsala, Sweden), connected to the NGC Chromatography System (Bio-Rad Laboratories, Hercules, CA, USA). The mobile phase used in SEC was phosphate buffered saline (PBS) supplemented by 3% glycerol.

Expression vector of chimeric 5D3 was introduced in suspension culture of HEK-293T cells using linear polyethylene imine as described previously [93]. Five days after transfection, conditioned medium of the culture was harvested by sequential centrifugation at 500xg for 10 mins and 10 000xg for 30 mins, respectively. Supernatant was filtered by tangential flow filtration, mixed with preequilibrated protein A agarose (Pierce, Thermo Fisher Scientific) and

incubated 1 hour at RT. Agarose was then stringently washed by PBS supplemented with 1 mM EDTA and 10% glycerol. Protein was eluted by 100 mM glycine pH 2.7 and immediately neutralized. Chimeric 5D3 was filtered, flash frozen at concentration 2 mg/mL in liquid nitrogen and stored at -80°C until further use.

Thermal Stability by nanoDSF

Proteins at final concentration 0.3 mg/mL were subjected to a temperature gradient from 25 °C to 95 °C using a Prometheus NT.48 fluorimeter (NanoTemper Technologies, München, Germany). The melting temperature (Tm) was calculated from the first derivative of a fluorescence ratio emitted at 350 nm and 330 nm.

Determination of binding affinities

Harvesting of cells and the detection of interaction between an engager and a specific antigen was performed as described in **[50].** In short, cells were mixed with protein of interest in a total volume of 20 µL and incubated for 15 min at 4°C. Presence of 5D3-CP33 on the surface of cells was detected by sequential staining with the mouse monoclonal anti-Strep tag antibody (1 µg/mL, Immo, IBA; cat.no. 2-1517-001) and a goat anti-mouse secondary antibody conjugated to Alexa Fluor 647 (0.25 µg/mL; Thermo Fisher Scientific; cat.no. A-21236). Binding of 5D3-CP33 on HEK-293T-CD64 and HEK-293T cells was detected by Strep-TactinXT conjugated to DY-649 (0.1 µg/mL; Immo, IBA; cat.no. 2-1568-050). Bound ch5D3 was detected by goat anti-human secondary antibody conjugated to Alexa Fluor 647 (1 µg/mL; Thermo Fisher Scientific; cat.no. A-

21445). All incubations were carried out 15 minutes at 4°C followed by stringent washes. The fluorescence signal was acquired by BD LSRFortessa flow cytometer (BD Biosciences, San Jose, CA, USA). Data were analyzed using the FlowJo software (FlowJo, LLC, Ashland, OR, USA). Dissociation constants (K_D) for each arm were calculated in the GraphPad Prism software using a non-linear regression algorithm (GraphPad, San Diego CA, USA).

Quantification of ROS production

U937 monocytes were activated by 0.1 µg/mL IFN-γ overnight at 37 °C. Following incubation, 15 x 10^4 effectors were mixed with targets at the ratio 1:1 in a white 96-well U-bottom microplate (Nunc, Thermo Fischer, MA, USA), then 5D3-CP33 was added to cell suspension. Stock of lucigenin (1.2 mg/mL in RPMI-1640 media) was added to wells to reach final concentration 0.12 mg/mL, making a total volume of reactions 100 µL. The plate was centrifuged at 200xg 2 min and the chemiluminescence signal of lucigenin was measured in regular intervals (135 sec) for 45 minutes in a Clariostar microplate reader (BMG Labtech, Ortenberg, Germany) pre-heated to 37 °C.

Antibody-dependent cell-mediated phagocytosis

U937 effector monocytes were activated by 0.1 µg/mL IFN-γ overnight at 37 °C. The following day, monocytes and target cells were incubated with 1.9 µM Vybrant DiD Cell-Labelling solution and 5.7 µM DiO Cell Labelling solution (Thermo Fisher Scientific), respectively. Incubation run in serum-free RPMI-1640 media at 37 °C for 30 minutes in cell density 1 x 10^6 cells/mL. Following

incubation, cells were washed three times with RPMI-1640 media supplemented with 14% low IgG FBS (Gibco, Thermo Fisher Scientific). Target and effector cells were mixed in ratio 1:1 (total number 30 x 10^4 cells per well, total volume 75 uL) in 96-well U-bottom microplate. Cells were then mixed with 3-fold dilution series of 5D3-CP33 ranging from 1 µM to 0.15 nM in final volume 100 µL. The plate was centrifuged at 200xg for 2 min and incubated at 37 °C for 1 hour. Following incubation, the plate was cooled to 4°C and samples were analyzed with a BD LSR Fortessa flow cytometer.

In microscopy analysis, cell samples were processed by the same procedure described above. Prior imaging cells were dissolved in cooled FluoroBrite DMEM media (Thermo Fisher Scientific), applied onto glass coverslips precoated by poly-L-lysine and immediately analyzed by a Leica TCS SP8 confocal microscope (Leica, Wetzlar, Germany) equipped with a water immersion objective HC PL APO CS2 with magnification 63x. Microscope instrumentation was preequilibrated to 20°C. The set of images was acquired in z-axis at 2 µm intervals. Images were analyzed in Fiji [94] and processed in CS4 Photoshop software (Adobe Systems, San Jose, CA).

Abbreviations

ADA	anti-drug antibody
ADCP	antibody-dependent cell-mediated phagocytosis
BiTE	bispecific T-cell engager
CAR T	chimeric antigen T-cell receptor
CDC	cell-dependent cytotoxicity
Fc	crystallizable fragment of antibody

FcγRI	crystallizable fragment gamma receptor I
FDA	US Food and Drug Administration
GCPII	glutamate carboxypeptidase II
mAb	monoclonal antibody
mCRPC	metastatic castration-resistant prostate cancer
PCa	prostate cancer
PSA	prostate specific antigen
PSMA	prostate specific membrane antigen
ROS	reactive oxygen species
scFv	single chain variable fragment

Data availability

All data generated or analyzed during this study are included in this manuscript and its supplementary information file.

Acknowledgement

We thank I. Jelinkova for her outstanding technical assistance.

Author contributions

G.D., C.B. and Z.N. conceived the study. G.D., J.P., B.H. and J.N. performed experiments and ran data analysis. G.D., C.B., and Z.N. interpreted and presented the data. G.D. Z.N., and C.B. contributed to writing of manuscript.

Reference

1. Siegel RL, Miller KD, Wagle NS, Jemal A. Cancer statistics, 2023. CA Cancer J Clin. 2023;73(1):17-48.
2. Machulkin AE, Uspenskaya AA, Zyk NY, Nimenko EA, Ber AP, Petrov SA, et al. PSMA-targeted small-molecule docetaxel conjugate: Synthesis and preclinical evaluation. Eur J Med Chem. 2022;227:113936.
3. Afshar-Oromieh A, Malcher A, Eder M, Eisenhut M, Linhart HG, Hadaschik BA, et al. PET imaging with a [68Ga]gallium-labelled PSMA ligand for the diagnosis of prostate cancer: biodistribution in humans and first evaluation of tumour lesions. Eur J Nucl Med Mol Imaging. 2013;40(4):486-95.
4. Schmidkonz C, Hollweg C, Beck M, Reinfelder J, Goetz TI, Sanders JC, et al. (99m) Tc-MIP-1404-SPECT/CT for the detection of PSMA-positive lesions in 225 patients with biochemical recurrence of prostate cancer. Prostate. 2018;78(1):54-63.
5. Liolios C, Koutsikou TS, Salvanou EA, Kapiris F, Machairas E, Stampolaki M, et al. Synthesis and in vitro proof-of-concept studies on bispecific iron oxide magnetic nanoparticles targeting PSMA and GRP receptors for PET/MR imaging of prostate cancer. Int J Pharm. 2022;624:122008.
6. Zhang X, Qi S, Liu D, Du J, Jin J. PSMA-Targeted Supramolecular Nanoparticles Prepared From Cucurbit[8]uril-Based Ternary Host-Guest Recognition for Prostate Cancer Therapy. Front Chem. 2022;10:847523.
7. Barinka C, Rinnova M, Sacha P, Rojas C, Majer P, Slusher BS, et al. Substrate specificity, inhibition and enzymological analysis of recombinant human glutamate carboxypeptidase II. J Neurochem. 2002;80(3):477-87.
8. Berger UV, Carter RE, McKee M, Coyle JT. N-acetylated alpha-linked acidic dipeptidase is expressed by non-myelinating Schwann cells in the peripheral nervous system. Journal of Neurocytology.99-109.
9. Chang SS, Reuter VE, Heston WDW, Bander NH, Grauer LS, Gaudin PB. Five Different Anti-Prostate-specific Membrane Antigen (PSMA) Antibodies Confirm PSMA Expression in Tumor-associated Neovasculature. Cancer Res.59(13):3192–8.
10. Kinoshita Y, Kuratsukuri K, Landas S, Imaida K, Rovito PM, Jr., Wang CY, et al. Expression of prostate-specific membrane antigen in normal and malignant human tissues. World J Surg. 2006;30(4):628-36.
11. Sokoloff RL, Norton KC, Gasior CL, Marker KM, Grauer LS. A dual-monoclonal sandwich assay for prostate-specific membrane antigen: Levels in tissues, seminal fluid and urine. The Prostate. 2000;43(2):150-7.
12. Barinka C, Rojas C, Slusher B, Pomper M. Glutamate Carboxypeptidase II in Diagnosis and Treatment of Neurologic Disorders and Prostate Cancer. Curr Med Chem. 2012;19(6):856-70.
13. Barinka C, Starkova J, Konvalinka J, Lubkowski J. A high-resolution structure of ligand-free human glutamate carboxypeptidase II. Acta Crystallogr Sect F Struct Biol Cryst Commun. 2007;63(Pt 3):150-3.
14. Meller B, Bremmer F, Sahlmann CO, Hijazi S, Bouter C, Trojan L, et al. Alterations in androgen deprivation enhanced prostate-specific membrane antigen (PSMA) expression in prostate cancer cells as a target for diagnostics and therapy. EJNMMI Res. 2015;5(1):66.

15. Novakova Z, Cerny J, Choy CJ, Nedrow JR, Choi JK, Lubkowski J, et al. Design of composite inhibitors targeting glutamate carboxypeptidase II: the importance of effector functionalities. FEBS J. 2016;283(1):130-43.
16. Ganguly T, Dannoon S, Hopkins MR, Murphy S, Cahaya H, Blecha JE, et al. A high-affinity [(18)F]-labeled phosphoramidate peptidomimetic PSMA-targeted inhibitor for PET imaging of prostate cancer. Nucl Med Biol. 2015;42(10):780-7.
17. Barinka C, Hlouchova K, Rovenska M, Majer P, Dauter M, Hin N, et al. Structural basis of interactions between human glutamate carboxypeptidase II and its substrate analogs. J Mol Biol. 2008;376(5):1438-50.
18. Farolfi A, Calderoni L, Mattana F, Mei R, Telo S, Fanti S, et al. Current and Emerging Clinical Applications of PSMA PET Diagnostic Imaging for Prostate Cancer. J Nucl Med. 2021;62(5):596-604.
19. Afshar-Oromieh A, Babich JW, Kratochwil C, Giesel FL, Eisenhut M, Kopka K, et al. The Rise of PSMA Ligands for Diagnosis and Therapy of Prostate Cancer. J Nucl Med. 2016;57(Suppl 3):79S-89S.
20. Fay EK, Graff JN. Immunotherapy in Prostate Cancer. Cancers (Basel). 2020;12(7).
21. Sundar R, Cho BC, Brahmer JR, Soo RA. Nivolumab in NSCLC: latest evidence and clinical potential. Ther Adv Med Oncol. 2015;7(2):85-96.
22. Jen EY, Xu Q, Schetter A, Przepiorka D, Shen YL, Roscoe D, et al. FDA Approval: Blinatumomab for Patients with B-cell Precursor Acute Lymphoblastic Leukemia in Morphologic Remission with Minimal Residual Disease. Clin Cancer Res. 2019;25(2):473-7.
23. Pai-Scherf L, Blumenthal GM, Li H, Subramaniam S, Mishra-Kalyani PS, He K, et al. FDA Approval Summary: Pembrolizumab for Treatment of Metastatic Non-Small Cell Lung Cancer: First-Line Therapy and Beyond. Oncologist. 2017;22(11):1392-9.
24. King A. Could immunotherapy finally break through in prostate cancer? Nature. 2022;609(7927):S42-S4.
25. Kantoff PW, Higano CS, Shore ND, Berger ER, Small EJ, Penson DF, et al. Sipuleucel-T Immunotherapy for Castration-Resistant Prostate Cancer. N Engl J Med.363(5):411-22.
26. Kantoff PW, Schuetz TJ, Blumenstein BA, Glode LM, Bilhartz DL, Wyand M, et al. Overall survival analysis of a phase II randomized controlled trial of a Poxviral-based PSA-targeted immunotherapy in metastatic castration-resistant prostate cancer. J Clin Oncol. 2010;28(7):1099-105.
27. Gulley JL, Arlen PM, Tsang KY, Yokokawa J, Palena C, Poole DJ, et al. Pilot study of vaccination with recombinant CEA-MUC-1-TRICOM poxviral-based vaccines in patients with metastatic carcinoma. Clin Cancer Res. 2008;14(10):3060-9.
28. Lubaroff DM, Konety BR, Link B, Gerstbrein J, Madsen T, Shannon M, et al. Phase I clinical trial of an adenovirus/prostate-specific antigen vaccine for prostate cancer: safety and immunologic results. Clin Cancer Res. 2009;15(23):7375-80.
29. Handa S, Hans B, Goel S, Bashorun HO, Dovey Z, Tewari A. Immunotherapy in prostate cancer: current state and future perspectives. Ther Adv Urol. 2020;12:1756287220951404.
30. Kwon ED, Drake CG, Scher HI, Fizazi K, Bossi A, van den Eertwegh AJ, et al. Ipilimumab versus placebo after radiotherapy in patients with metastatic castration-resistant prostate cancer that had progressed after docetaxel chemotherapy (CA184-043): a multicentre, randomised, double-blind, phase 3 trial. Lancet Oncol. 2014;15(7):700-12.
31. Small EJ, Tchekmedyian NS, Rini BI, Fong L, Lowy I, Allison JP. A pilot trial of CTLA-4 blockade with human anti-CTLA-4 in patients with hormone-refractory prostate cancer. Clin Cancer Res. 2007;13(6):1810-5.
32. Hlouchova K, Barinka C, Konvalinka J, Lubkowski J. Structural insight into the evolutionary and pharmacologic homology of glutamate carboxypeptidases II and III. FEBS J. 2009;276(16):4448-62.

533 33. Zhang W, Ran S, Sambade M, Huang X, Thorpe PE. A monoclonal antibody that blocks VEGF
534 binding to VEGFR2 (KDR/Flk-1) inhibits vascular expression of Flk-1 and tumor growth in an orthotopic
535 human breast cancer model. Angiogenesis. 2002;5:35-44.
536 34. Gao Y. Complement system in Anti-CD20 mAb therapy for cancer: A mini-review. Int J
537 Immunopathol Pharmacol. 2023;37:3946320231181464.
538 35. Petricevic B, Laengle J, Singer J, Sachet M, Fazekas J, Steger G, et al. Trastuzumab mediates
539 antibody-dependent cell-mediated cytotoxicity and phagocytosis to the same extent in both adjuvant and
540 metastatic HER2/neu breast cancer patients. J Transl Med. 2013;11:307.
541 36. Shrestha P, Astter Y, Davis DA, Zhou T, Yuan CM, Ramaswami R, et al. Daratumumab induces cell-
542 mediated cytotoxicity of primary effusion lymphoma and is active against refractory disease.
543 Oncoimmunology. 2023;12(1):2163784.
544 37. Van Wagoner CM, Rivera-Escalera F, Jaimes-Delgadillo NC, Chu CC, Zent CS, Elliott MR. Antibody-
545 mediated phagocytosis in cancer immunotherapy. Immunol Rev. 2023;319(1):128-41.
546 38. Ma X, Wong SW, Zhou P, Chaulagain CP, Doshi P, Klein AK, et al. Daratumumab binds to mobilized
547 CD34+ cells of myeloma patients in vitro without cytotoxicity or impaired progenitor cell growth. Exp
548 Hematol Oncol. 2018;7:27.
549 39. Naicker SD, Feerick CL, Lynch K, Swan D, McEllistrim C, Henderson R, et al. Cyclophosphamide
550 alters the tumor cell secretome to potentiate the anti-myeloma activity of daratumumab through
551 augmentation of macrophage-mediated antibody dependent cellular phagocytosis. Oncoimmunology.
552 2021;10(1):1859263.
553 40. Sanchez L, Wang Y, Siegel DS, Wang ML. Daratumumab: a first-in-class CD38 monoclonal antibody
554 for the treatment of multiple myeloma. J Hematol Oncol. 2016;9(1):51.
555 41. Shi Y, Fan X, Deng H, Brezski RJ, Rycyzyn M, Jordan RE, et al. Trastuzumab triggers phagocytic
556 killing of high HER2 cancer cells in vitro and in vivo by interaction with Fcgamma receptors on
557 macrophages. J Immunol. 2015;194(9):4379-86.
558 42. van de Donk N, Usmani SZ. CD38 Antibodies in Multiple Myeloma: Mechanisms of Action and
559 Modes of Resistance. Front Immunol. 2018;9:2134.
560 43. Zahavi D, Weiner L. Monoclonal Antibodies in Cancer Therapy. Antibodies (Basel). 2020;9(3).
561 44. Cha HR, Lee JH, Ponnazhagan S. Revisiting Immunotherapy: A Focus on Prostate Cancer. Cancer
562 Res. 2020;80(8):1615-23.
563 45. Zuccolotto G, Penna A, Fracasso G, Carpanese D, Montagner IM, Dalla Santa S, et al. PSMA-Specific
564 CAR-Engineered T Cells for Prostate Cancer: CD28 Outperforms Combined CD28-4-1BB "Super-
565 Stimulation". Front Oncol. 2021;11:708073.
566 46. Brischwein K, Schlereth B, Guller B, Steiger C, Wolf A, Lutterbuese R, et al. MT110: a novel
567 bispecific single-chain antibody construct with high efficacy in eradicating established tumors. Mol
568 Immunol. 2006;43(8):1129-43.
569 47. Hummel H-D, Kufer P, Grüllich C, Seggewiss-Bernhardt R, Deschler-Baier B, Chatterjee M, et al.
570 Pasotuxizumab, a BiTE® immune therapy for castration-resistant prostate cancer: Phase I, dose-escalation
571 study findings. Immunotherapy. 2020;13.
572 48. Minn I, Huss DJ, Ahn H-H, Chinn TM, Park A, Jones J, et al. Imaging CAR T cell therapy with PSMA-
573 targeted positron emission tomography. Sci Adv. 2019;5(7):eaaw5096.
574 49. Das G, Ptacek J, Havlinova B, Nedvedova J, Barinka C, Novakova Z. Targeting Prostate Cancer Using
575 Bispecific T-Cell Engagers against Prostate-Specific Membrane Antigen. ACS Pharmacology & Translational
576 Science. 2023;6(11):1703-14.
577 50. Novakova Z, Belousova N, Foss CA, Havlinova B, Gresova M, Das G, et al. Engineered Fragments
578 of the PSMA-Specific 5D3 Antibody and Their Functional Characterization. Int J Mol Sci. 2020;21(18):6672.

51. Bonetto S, Spadola L, Buchanan AG, Jermutus L, Lund J. Identification of cyclic peptides able to mimic the functional epitope of IgG1-Fc for human Fc gammaRI. FASEB J. 2009;23(2):575-85.
52. Ito T, Tsumoto K. Effects of subclass change on the structural stability of chimeric, humanized, and human antibodies under thermal stress. Protein Sci. 2013;22(11):1542-51.
53. Akinrinmade OA, Chetty S, Daramola AK, Islam MU, Thepen T, Barth S. CD64: An Attractive Immunotherapeutic Target for M1-type Macrophage Mediated Chronic Inflammatory Diseases. Biomedicines. 2017;5(3):56.
54. Boinapally S, Ahn HH, Cheng B, Brummet M, Nam H, Gabrielson KL, et al. A prostate-specific membrane antigen (PSMA)-targeted prodrug with a favorable in vivo toxicity profile. Sci Rep. 2021;11(1):7114.
55. Weiskopf K, Weissman IL. Macrophages are critical effectors of antibody therapies for cancer. MAbs. 2015;7(2):303-10.
56. Poh AR, Ernst M. Targeting Macrophages in Cancer: From Bench to Bedside. Front Oncol. 2018;8:49.
57. Yang Q, Guo N, Zhou Y, Chen J, Wei Q, Han M. The role of tumor-associated macrophages (TAMs) in tumor progression and relevant advance in targeted therapy. Acta Pharm Sin B. 2020;10(11):2156-70.
58. Petty AJ, Yang Y. Tumor-associated macrophages: implications in cancer immunotherapy. Immunotherapy. 2017;9(3):289-302.
59. DeNardo DG, Ruffell B. Macrophages as regulators of tumour immunity and immunotherapy. Nat Rev Immunol. 2019;19(6):369-82.
60. Dallavalasa S, Beeraka NM, Basavaraju CG, Tulimilli SV, Sadhu SP, Rajesh K, et al. The Role of Tumor Associated Macrophages (TAMs) in Cancer Progression, Chemoresistance, Angiogenesis and Metastasis - Current Status. Curr Med Chem. 2021;28(39):8203-36.
61. He Z, Zhang S. Tumor-Associated Macrophages and Their Functional Transformation in the Hypoxic Tumor Microenvironment. Front Immunol. 2021;12:741305.
62. Goswami S, Anandhan S, Raychaudhuri D, Sharma P. Myeloid cell-targeted therapies for solid tumours. Nat Rev Immunol. 2023;23(2):106-20.
63. Mancardi DA, Albanesi M, Jonsson F, Iannascoli B, Van Rooijen N, Kang X, et al. The high-affinity human IgG receptor FcgammaRI (CD64) promotes IgG-mediated inflammation, anaphylaxis, and antitumor immunotherapy. Blood. 2013;121(9):1563-73.
64. Nywening TM, Belt BA, Cullinan DR, Panni RZ, Han BJ, Sanford DE, et al. Targeting both tumour-associated CXCR2(+) neutrophils and CCR2(+) macrophages disrupts myeloid recruitment and improves chemotherapeutic responses in pancreatic ductal adenocarcinoma. Gut. 2018;67(6):1112-23.
65. Singh S, Barik D, Arukha AP, Prasad S, Mohapatra I, Singh A, et al. Small Molecule Targeting Immune Cells: A Novel Approach for Cancer Treatment. Biomedicines. 2023;11(10):2621.
66. Mitchem JB, Brennan DJ, Knolhoff BL, Belt BA, Zhu Y, Sanford DE, et al. Targeting tumor-infiltrating macrophages decreases tumor-initiating cells, relieves immunosuppression, and improves chemotherapeutic responses. Cancer Res. 2013;73(3):1128-41.
67. Chen Y, Yu Z, Tan X, Jiang H, Xu Z, Fang Y, et al. CAR-macrophage: A new immunotherapy candidate against solid tumors. Biomed Pharmacother. 2021;139:111605.
68. Zhang W, Liu L, Su H, Liu Q, Shen J, Dai H, et al. Chimeric antigen receptor macrophage therapy for breast tumours mediated by targeting the tumour extracellular matrix. Br J Cancer. 2019;121(10):837-45.
69. Chen C, Jing W, Chen Y, Wang G, Abdalla M, Gao L, et al. Intracavity generation of glioma stem cell–specific CAR macrophages primes locoregional immunity for postoperative glioblastoma therapy. SCIENCE TRANSLATIONAL MEDICINE. 2022;14(656):eabn1128.

70. Huo Y, Zhang H, Sa L, Zheng W, He Y, Lyu H, et al. M1 polarization enhances the antitumor activity of chimeric antigen receptor macrophages in solid tumors. J Transl Med. 2023;21(1):225.
71. Hadiloo K, Taremi S, Heidari M, Esmaeilzadeh A. The CAR macrophage cells, a novel generation of chimeric antigen-based approach against solid tumors. Biomark Res. 2023;11(1):103.
72. Lyadova I, Gerasimova T, Nenasheva T. Macrophages Derived From Human Induced Pluripotent Stem Cells: The Diversity of Protocols, Future Prospects, and Outstanding Questions. Front Cell Dev Biol. 2021;9:640703.
73. Klichinsky M, Ruella M, Shestova O, Lu XM, Best A, Zeeman M, et al. Human chimeric antigen receptor macrophages for cancer immunotherapy. Nat Biotechnol. 2020;38(8):947-53.
74. Olazabal IM, Martin-Cofreces NB, Mittelbrunn M, Martinez del Hoyo G, Alarcon B, Sanchez-Madrid F. Activation outcomes induced in naive CD8 T-cells by macrophages primed via "phagocytic" and nonphagocytic pathways. Mol Biol Cell. 2008;19(2):701-10.
75. Pratt KP. Anti-Drug Antibodies: Emerging Approaches to Predict, Reduce or Reverse Biotherapeutic Immunogenicity. Antibodies (Basel). 2018;7(2):19.
76. Suh K, Kyei I, Hage DS. Approaches for the detection and analysis of antidrug antibodies to biopharmaceuticals: A review. J Sep Sci. 2022;45(12):2077-92.
77. Yokota T, Milenic DE, Whitlow M, Schlom J. Rapid Tumor Penetration of a Single-Chain Fv and Comparison with Other Immunoglobulin Forms. Cancer Res. 1992;52(12):3402–8.
78. Munoz-Lopez P, Ribas-Aparicio RM, Becerra-Baez EI, Fraga-Perez K, Flores-Martinez LF, Mateos-Chavez AA, et al. Single-Chain Fragment Variable: Recent Progress in Cancer Diagnosis and Therapy. Cancers (Basel). 2022;14(17):4206.
79. Chames P, Van Regenmortel M, Weiss E, Baty D. Therapeutic antibodies: successes, limitations and hopes for the future. Br J Pharmacol. 2009;157(2):220-33.
80. Saxena A, Wu D. Advances in Therapeutic Fc Engineering - Modulation of IgG-Associated Effector Functions and Serum Half-life. Front Immunol. 2016;7:580.
81. Shen Y, Li H, Zhao L, Li G, Chen B, Guo Q, et al. Increased half-life and enhanced potency of Fc-modified human PCSK9 monoclonal antibodies in primates. PLoS One. 2017;12(8):e0183326.
82. Sondermann P, Szymkowski DE. Harnessing Fc receptor biology in the design of therapeutic antibodies. Curr Opin Immunol. 2016;40:78-87.
83. Santos MLd, Quintilio W, Manieri TM, Tsuruta LR, Moro AM. Advances and challenges in therapeutic monoclonal antibodies drug development. Brazilian Journal of Pharmaceutical Sciences. 2018;54(spe):e01007.
84. Harper T, Sharma A, Kaliyaperumal S, Fajardo F, Hsu K, Liu L, et al. Characterization of an Anti-CD70 Half-Life Extended Bispecific T-Cell Engager (HLE-BiTE) and Associated On-Target Toxicity in Cynomolgus Monkeys. Toxicol Sci. 2022;189(1):32-50.
85. Mandrup OA, Ong SC, Lykkemark S, Dinesen A, Rudnik-Jansen I, Dagnaes-Hansen NF, et al. Programmable half-life and anti-tumour effects of bispecific T-cell engager-albumin fusions with tuned FcRn affinity. Commun Biol. 2021;4(1):310.
86. Schlapschy M, Binder U, Borger C, Theobald I, Wachinger K, Kisling S, et al. PASylation: a biological alternative to PEGylation for extending the plasma half-life of pharmaceutically active proteins. Protein Eng Des Sel. 2013;26(8):489-501.
87. Mester S, Evers M, Meyer S, Nilsen J, Greiff V, Sandlie I, et al. Extended plasma half-life of albumin-binding domain fused human IgA upon pH-dependent albumin engagement of human FcRn in vitro and in vivo. MAbs. 2021;13(1):1893888.
88. McEnaney PJ, Fitzgerald KJ, Zhang AX, Douglass EF, Jr., Shan W, Balog A, et al. Chemically synthesized molecules with the targeting and effector functions of antibodies. J Am Chem Soc. 2014;136(52):18034-43.

672 89. Kopka K, Benesova M, Barinka C, Haberkorn U, Babich J. Glu-Ureido-Based Inhibitors of Prostate-
673 Specific Membrane Antigen: Lessons Learned During the Development of a Novel Class of Low-Molecular-
674 Weight Theranostic Radiotracers. J Nucl Med. 2017;58(Suppl 2):17S-26S.
675 90. García-García E, Rosales C. Fc Receptor Signaling in Leukocytes: Role in Host Defense and Immune
676 Regulation. Curr Immunol Rev. 2009;5(3):227-42.
677 91. Bakht MK, Hayward JJ, Shahbazi-Raz F, Skubal M, Tamura R, Stringer KF, et al. Identification of
678 alternative protein targets of glutamate-ureido-lysine associated with PSMA tracer uptake in prostate
679 cancer cells. Proc Natl Acad Sci U S A. 2022;119(4):e2025710119.
680 92. Dodev TS, Karagiannis P, Gilbert AE, Josephs DH, Bowen H, James LK, et al. A tool kit for rapid
681 cloning and expression of recombinant antibodies. Sci Rep. 2014;4:5885.
682 93. Skultetyova L, Ustinova K, Kutil Z, Novakova Z, Pavlicek J, Mikesova J, et al. Human histone
683 deacetylase 6 shows strong preference for tubulin dimers over assembled microtubules. Sci Rep.
684 2017;7(1):11547.
685 94. Schindelin J, Arganda-Carreras I, Frise E, Kaynig V, Longair M, Pietzsch T, et al. Fiji: an open-source
686 platform for biological-image analysis. Nat Methods. 2012;9(7):676-82.
687

688 # Supporting Information

689 S1 Table. List of primers

690 S1 Fig Sequence of 5D3/CP33 constructs

691 S2 Fig Microscopy images of phagocytosis

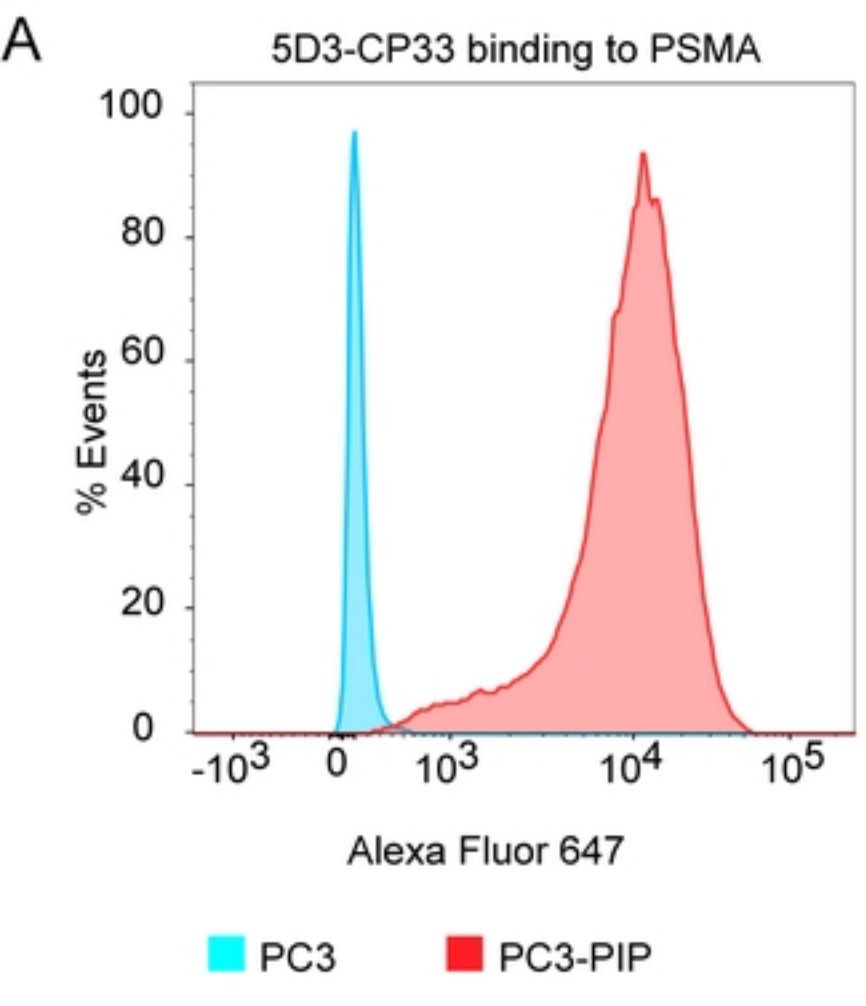

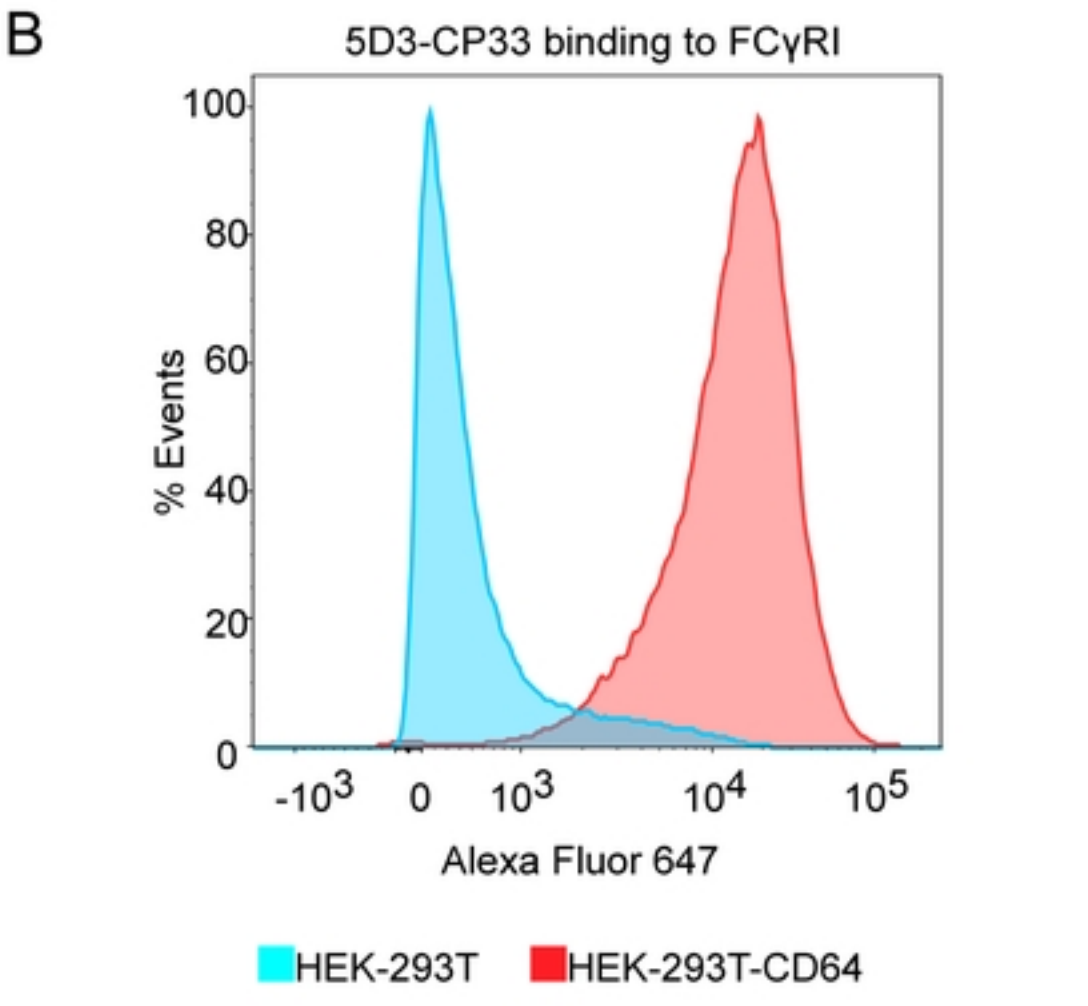

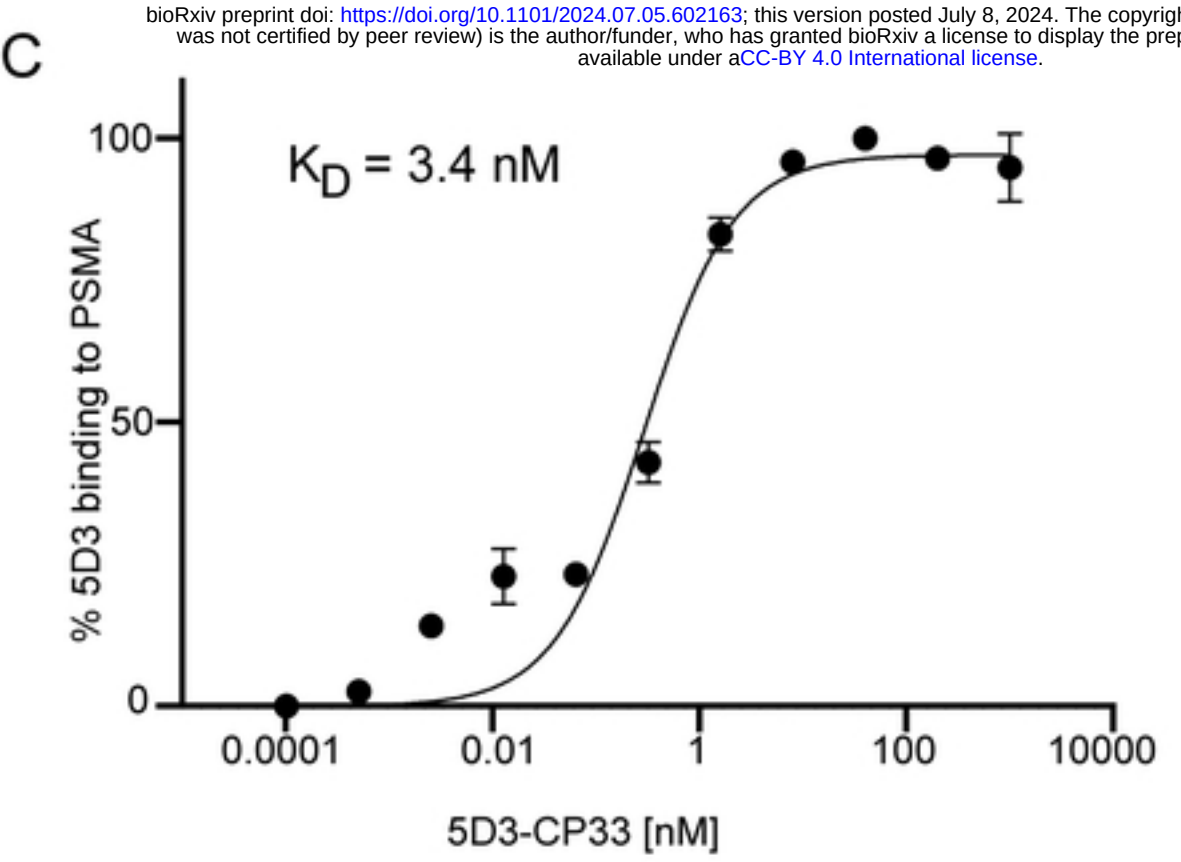

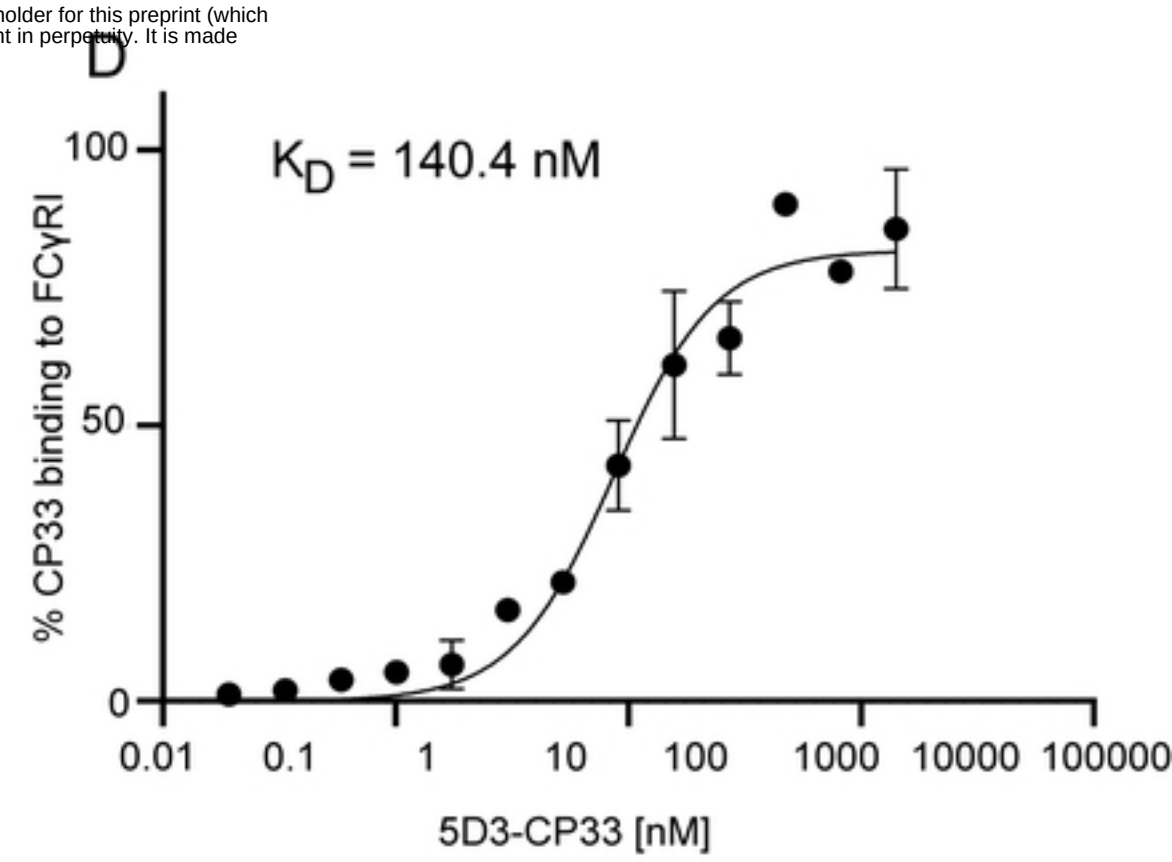

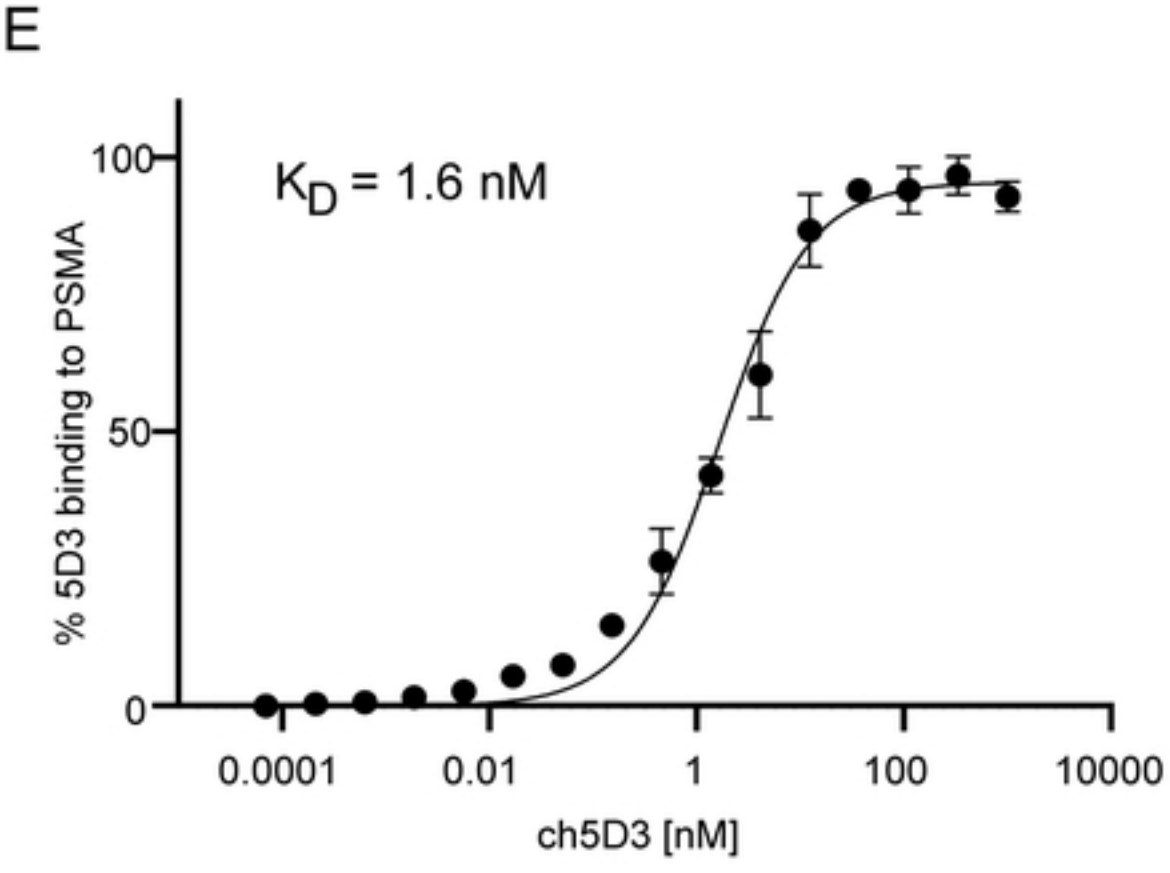

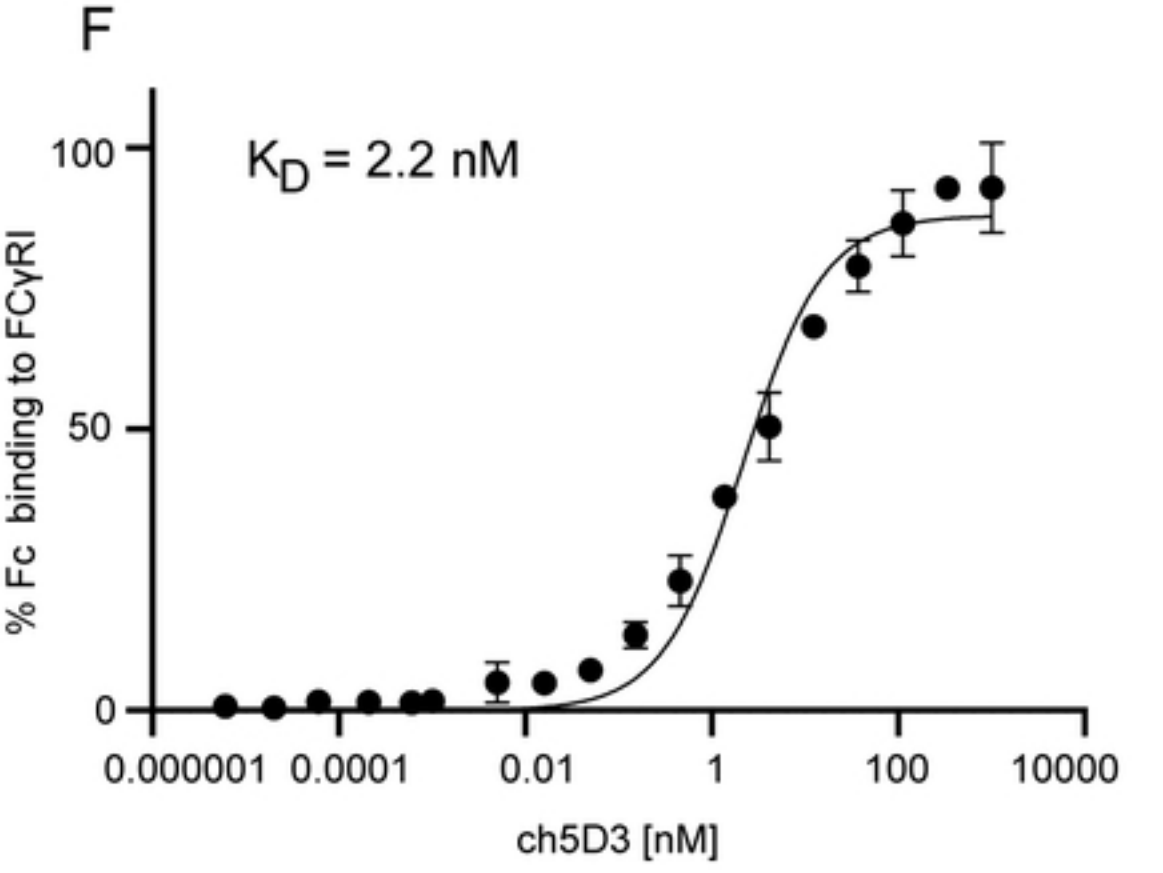

Figure 2

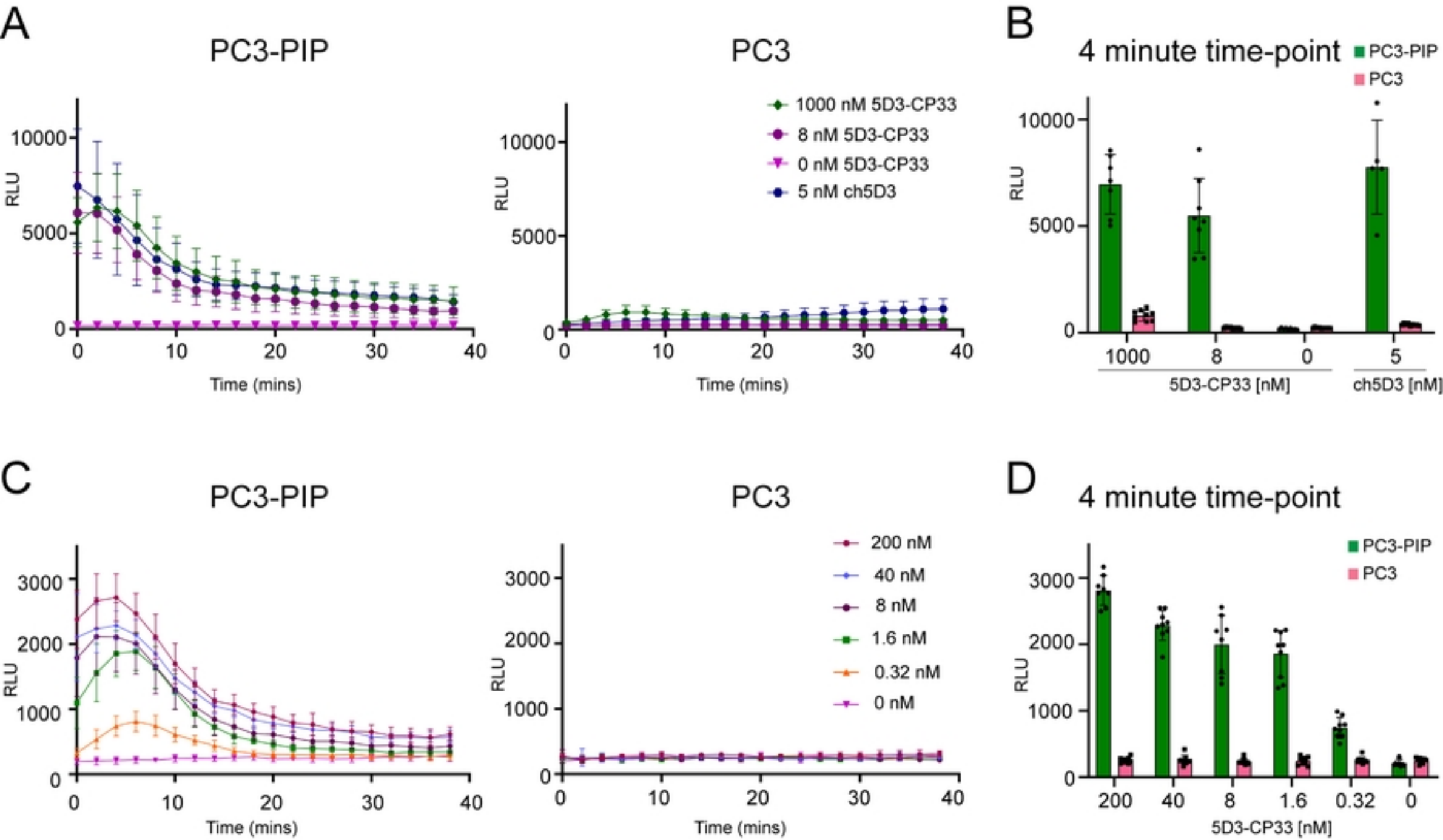
A
PC3-PIP
PC3
1000 nM 5D3-CP33
8 nM 5D3-CP33
0 nM 5D3-CP33
5 nM ch5D3
RLU
Time (mins)
B
4 minute time-point
PC3-PIP
PC3
RLU
1000
8
0
5
5D3-CP33 [nM]
ch5D3 [nM]
C
PC3-PIP
PC3
200 nM
40 nM
8 nM
1.6 nM
0.32 nM
0 nM
RLU
Time (mins)
D
4 minute time-point
PC3-PIP
PC3
RLU
200
40
8
1.6
0.32
0
5D3-CP33 [nM]

Figure 3

A

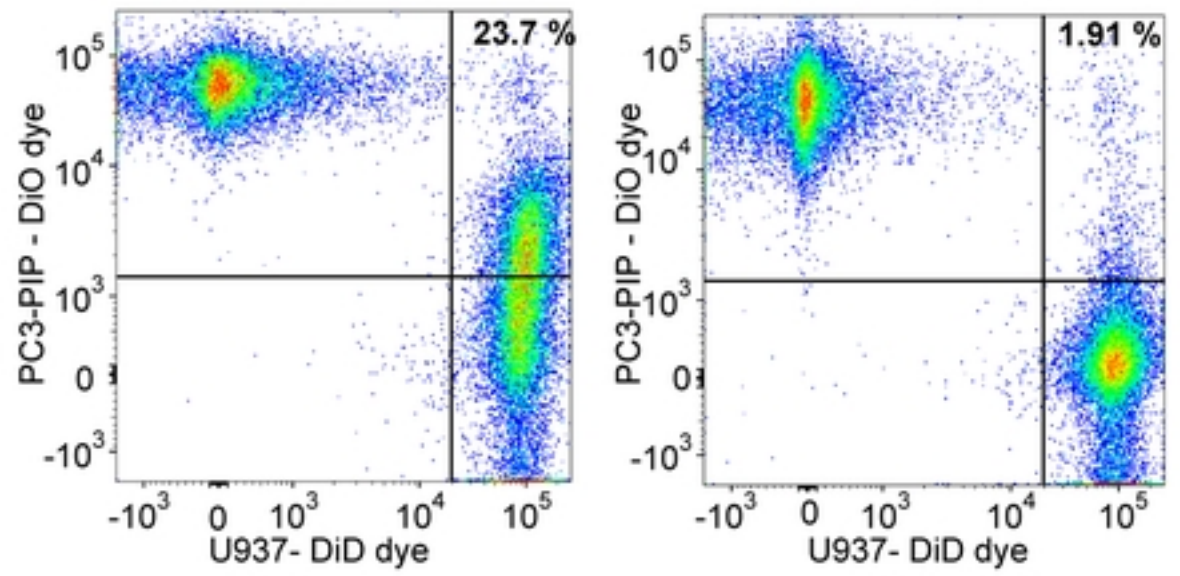
PC3-PIP cells
111 nM 5D3-CP33
no 5D3-CP33
23.7 %
1.91 %
PC3-PIP - DiO dye
U937- DiD dye

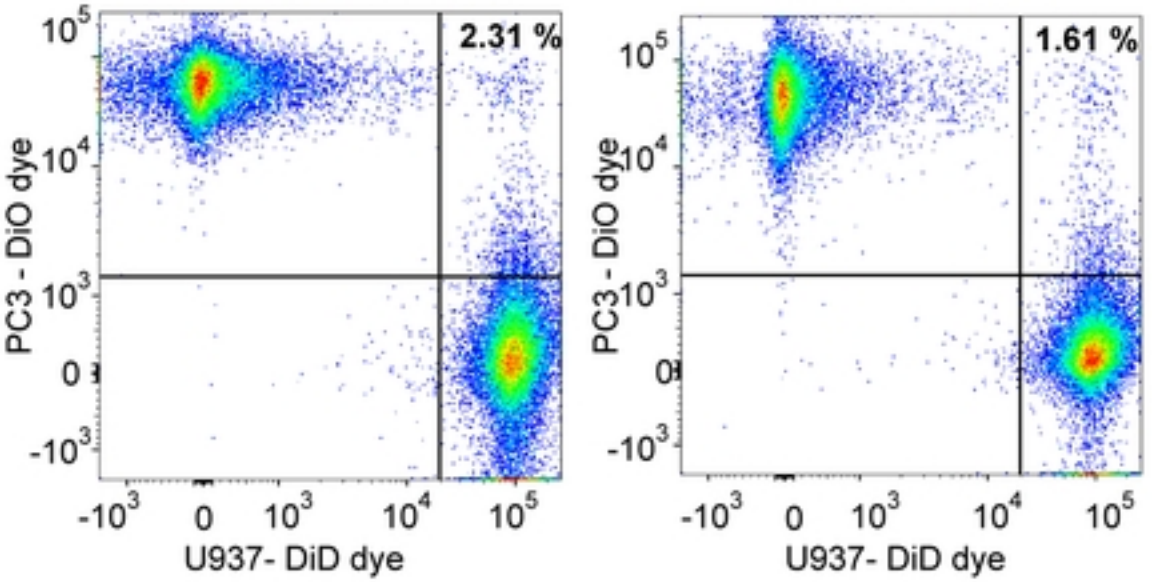
PC3 cells
111 nM 5D3-CP33
no 5D3-CP33
2.31 %
1.61 %
PC3 - DiO dye
U937- DiD dye

B

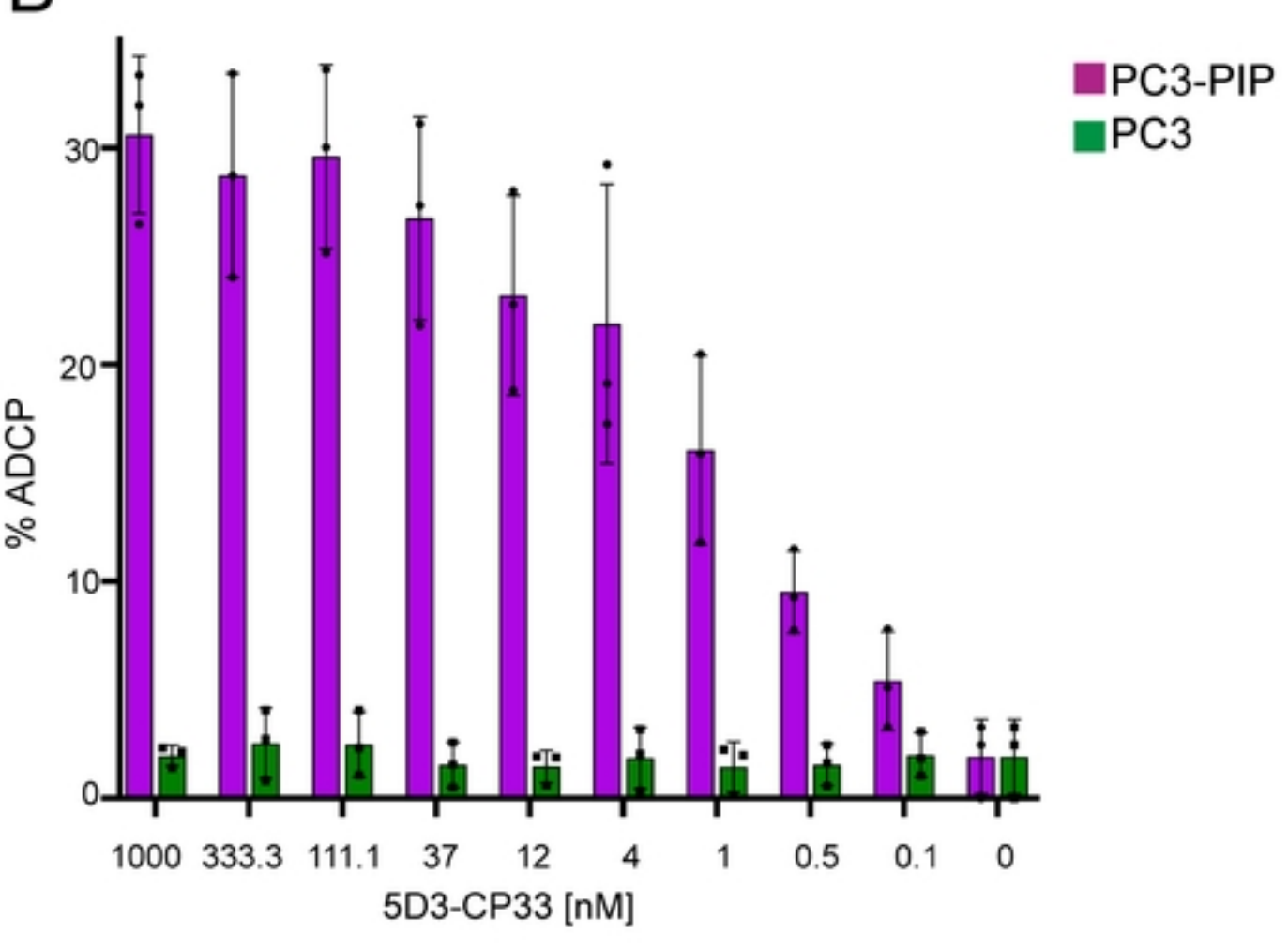
PC3-PIP
PC3
% ADCP
1000
333.3
111.1
37
12
4
1
0.5
0.1
0
5D3-CP33 [nM]

C

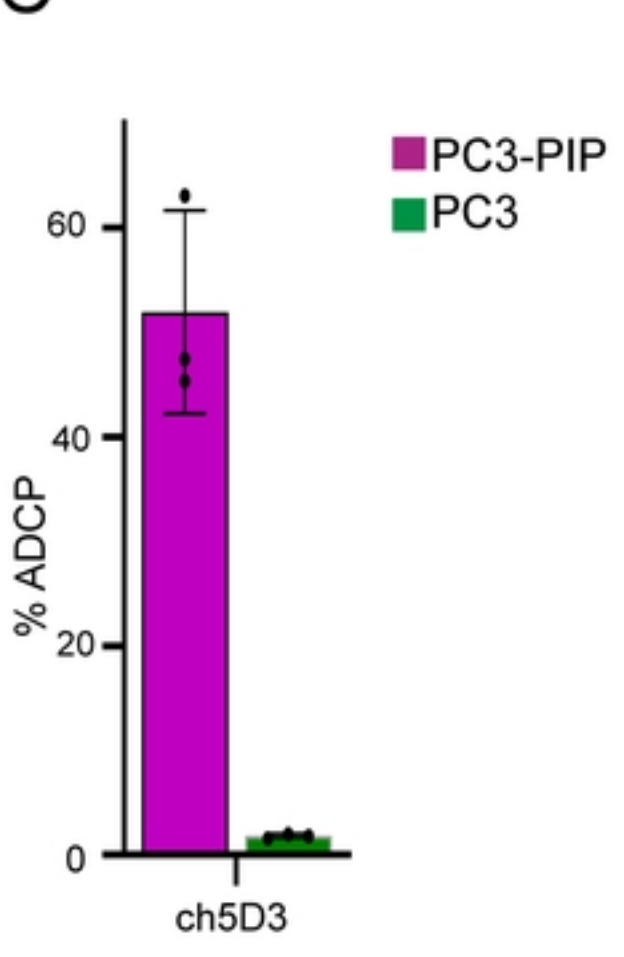
PC3-PIP
PC3
% ADCP
ch5D3

Figure 4

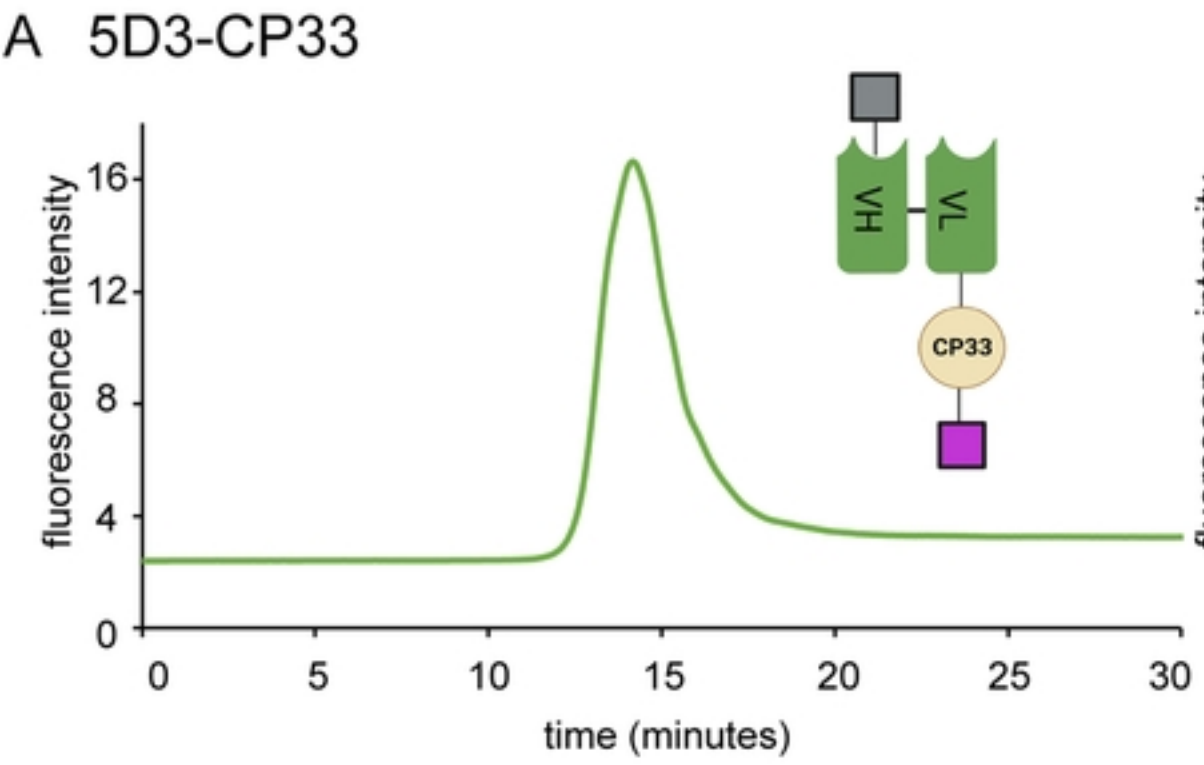

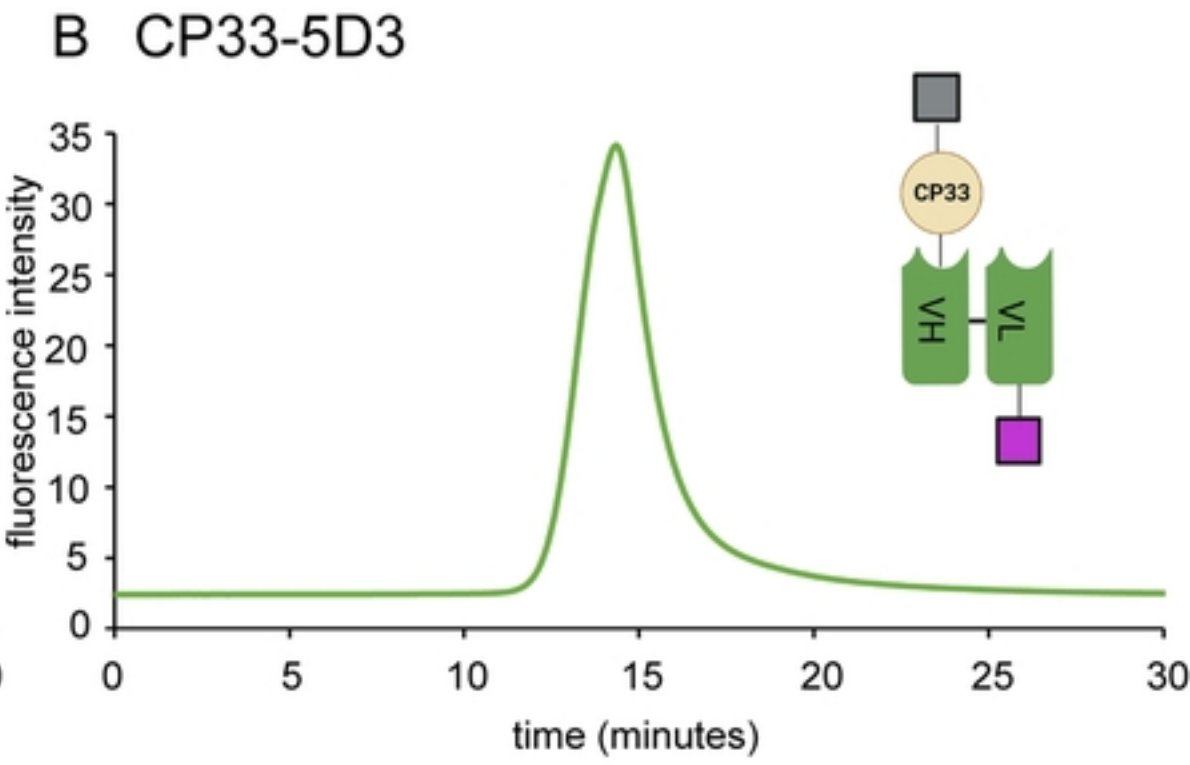

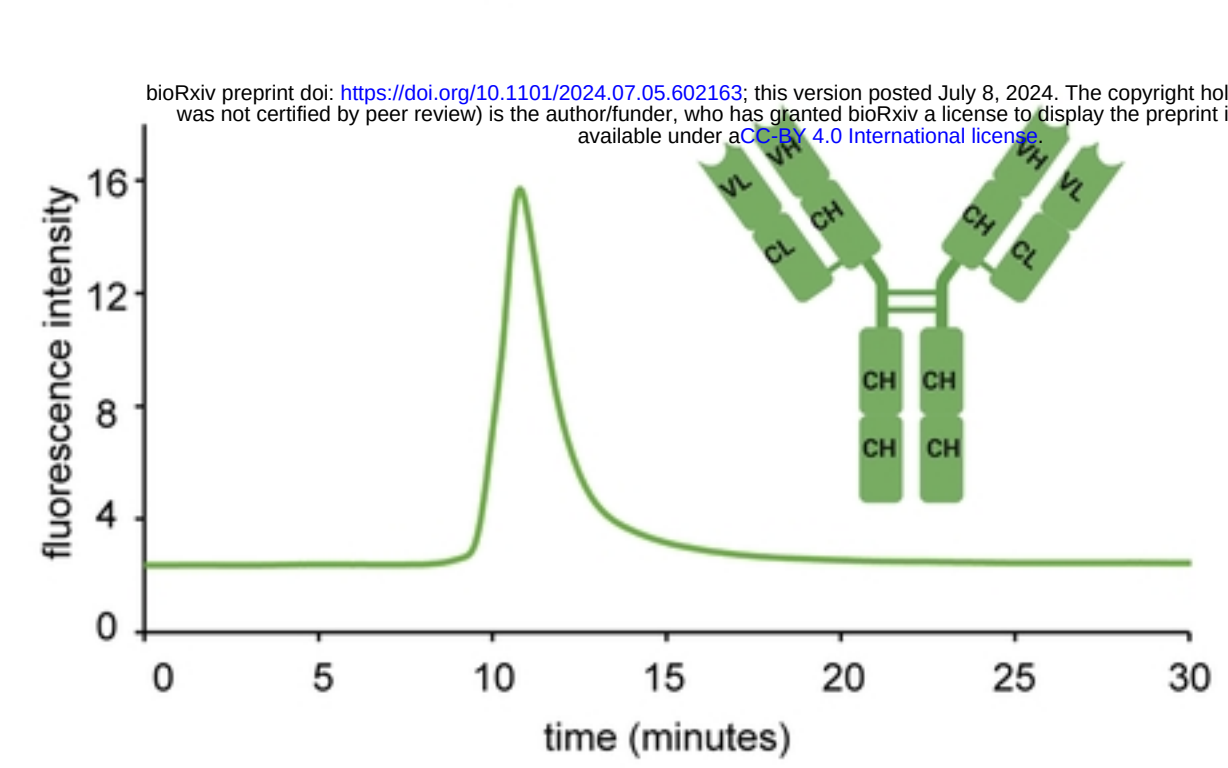

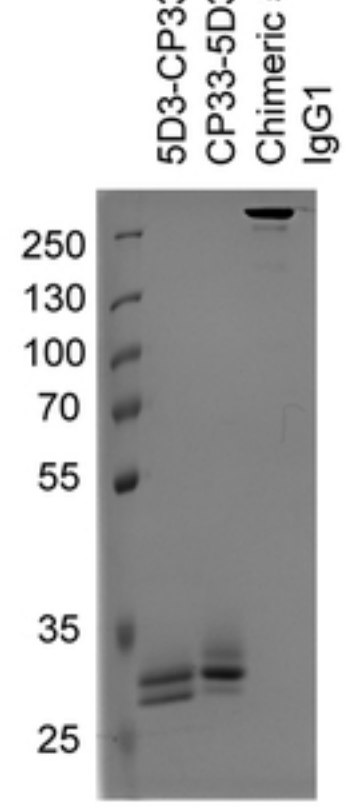

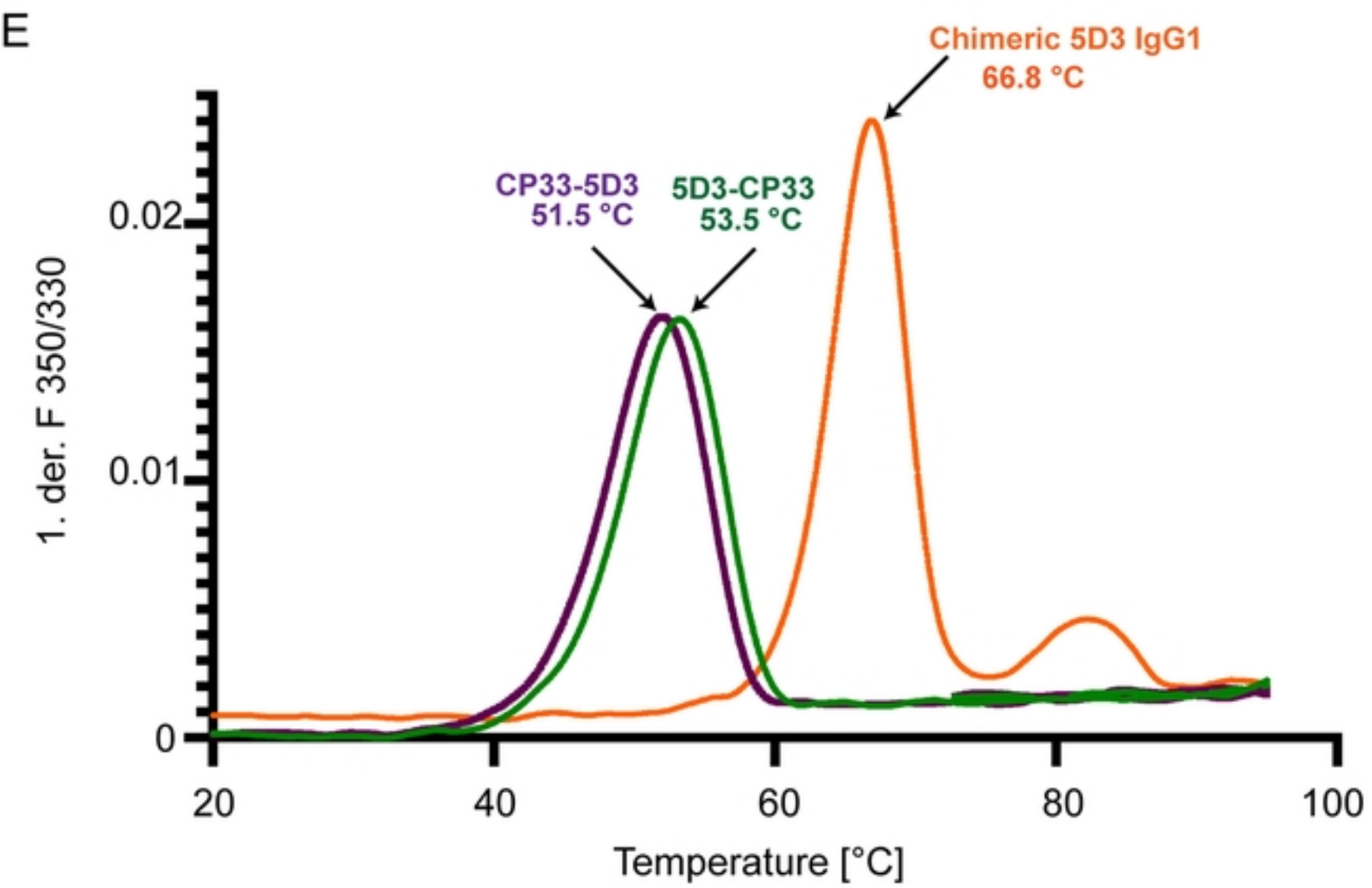

Figure 1